Open-Loop Active Load-Pull Setup Using the ZCU216 Radio Frequency System-on-Chip

Citation for the original published paper (version of record):
Shilinkov, I., Maaskant, R., Lasser, G. (2025). Open-Loop Active Load-Pull Setup Using the ZCU216 Radio Frequency System-on-Chip. IEEE Microwave and Wireless Technology Letters, 35(12): 2121-2124. http://dx.doi.org/10.1109/LMWT.2025.3633956

Open-Loop Active Load–Pull Setup Using the ZCU216 Radio Frequency System-on-Chip

Iaroslav Shilinkov, *Graduate Student Member, IEEE*, Rob Maaskant, *Senior Member, IEEE*, and Gregor Lasser, *Senior Member, IEEE*

***Abstract*—A fully self-contained active open-loop load–pull measurement system based on a commercial radio frequency system-on-chip (RFSoC) evaluation board is presented. The proposed setup eliminates the need for external signal generators and vector network analyzers (VNAs) by leveraging the ZCU216's integrated high-speed DACs and ADCs. A simple and extensible calibration method is introduced to accurately synthesize arbitrary load impedances presented to the device under test (DUT). The system's flexibility is demonstrated through three measurement scenarios: return loss measurements of a 3-D-printed horn antenna and small-signal gain measurements of the commercial RF power amplifier (PA) QPA9501, utilizing the setup as a two-port VNA and active load–pull measurements of the same PA at 5.4 GHz. Measurements agree with E5071C VNA measurements, validating the system's effectiveness and highlighting the potential of RFSoC platforms as cost-effective, reconfigurable alternatives to traditional load–pull instrumentation.**

***Index Terms*—Active load–pull, large-signal characterization, open loop.**

I. Introduction

ANTENNA arrays are a foundational technology for emerging 6G wireless systems, particularly in massive MIMO [1]. These systems require many transceiver chains, each with its own power amplifier (PA), making PA efficiency a critical factor. Modern high-efficiency architectures, such as Doherty, help address this, but their performance is highly sensitive to the load impedance [2].

In real-world arrays, the load seen by each PA is dynamic, affected by mutual coupling and interactions with neighboring elements. To characterize PAs under such varying conditions, load–pull techniques are used [3], where the impedance presented to the device under test (DUT) is swept.

Load–pull systems can be categorized into passive and active types, depending on how the load impedance is synthesized. Passive systems, which rely on load tuners, suffer from limited impedance coverage. Active load–pull systems overcome these limitations by injecting controlled signals into the DUT output, enabling the synthesis of arbitrary impedances—even outside the Smith chart [4].

Received 31 August 2025; revised 18 October 2025 and 12 November 2025; accepted 12 November 2025. Date of publication 24 November 2025; date of current version 11 December 2025. This work was supported by Swedish Foundation for Strategic Research. *(Corresponding author: Iaroslav Shilinkov).*

Iaroslav Shilinkov and Rob Maaskant are with the Department of Electrical Engineering, Chalmers University of Technology, 41296 Gothenburg, Sweden (e-mail: iaroslav@chalmers.se).

Gregor Lasser is with the Department of Microtechnology and Nanoscience, Chalmers University of Technology, 41296 Gothenburg, Sweden.

Digital Object Identifier 10.1109/LMWT.2025.3633956

Active systems can be implemented in either closed-loop or open-loop configurations. Closed-loop architectures regenerate and reinject the DUT's output signal after amplification and phase adjustment. They are often complex to implement, prone to stability issues, and require more involved calibration procedures [5]. In contrast, the open-loop systems offer simpler implementation, stable, and are straightforward to calibrate.

Traditional load–pull setups often rely on expensive instruments, such as vector network analyzers (VNAs) and signal generators. While FPGA-based load–pull implementations have been demonstrated [6], they typically still require such external hardware. In contrast, this work presents a fully self-contained active open-loop load–pull system implemented on a single commercial radio frequency system-on-chip (RFSoC) evaluation board.

Our main contributions are summarized as follows.

1) We demonstrate a fully self-contained active load—pull measurement system based on a single RFSoC evaluation board.
2) We introduce a simple method for synthesizing arbitrary load impedances, requiring no prior characterization of the DUT.

The remainder of this letter is organized as follows. Section II describes the architecture of the proposed measurement system. Section III outlines the calibration procedures, including two-port SOLT calibration and an iterative load calibration technique. Section IV presents the example measurements in two regimes: VNA measurements of the return loss of the 3-D-printed horn antenna and small-signal gain measurements of the RF PA, and load—pull measurements of the same PA at 5.4 GHz. Finally, Section V concludes this letter and summarizes the main contributions.

II. Measurement Setup Description

The proposed load–pull system is built around the ZCU216 RFSoC evaluation board, which integrates high-speed 14-bit DACs and ADCs and is controlled from a PC (see Fig. 1 for a system schematic).

Signal generation is done with direct digital synthesis (DDS) at 8 GSPS (second Nyquist zone), with out-of-band images suppressed by VBFZ-5500-S+ 4.9–6.2-GHz bandpass filters. Reception uses undersampling at 2.5 GSPS, with the same bandpass filters.

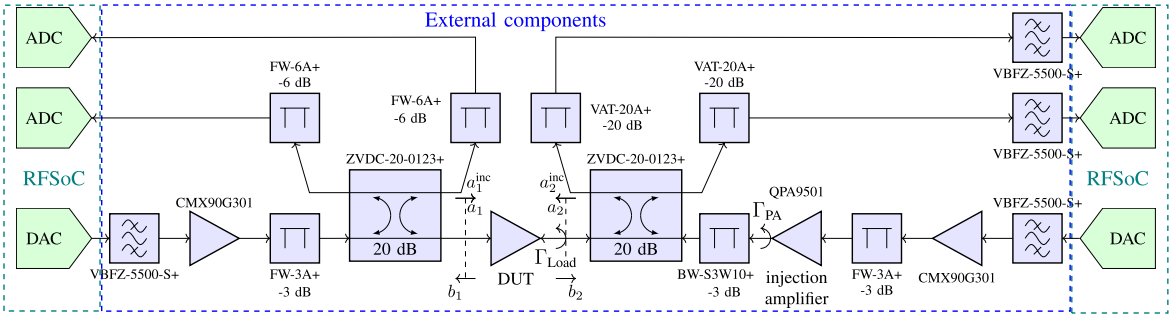

Fig. 1. Measurement setup schematic.

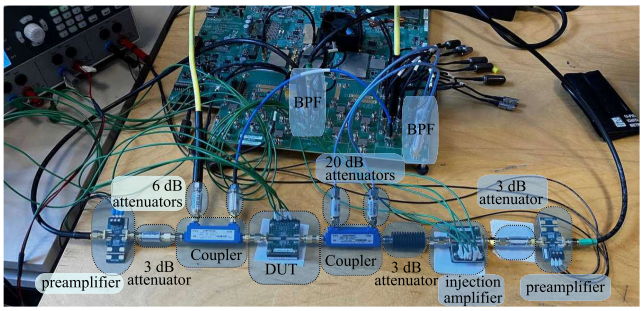

Fig. 2. Load–pull measurement setup photograph.

The RF signal path includes ZVDC-20-0123 + 1–20-GHz 20-dB directional couplers placed at the input and output of the DUT. Signal amplification is provided by CMX90G301 1.4–7.1-GHz, 15-dB gain blocks, which increase the drive levels before the DUT and the injection amplifier. The QPA9501 4.9–5.9-GHz RF PA is used both as the DUT and as the injection amplifier to synthesize controlled reflections. It has typical 32 dB of gain and 31.1-dBm P1dB. After the gain blocks FW-3A+, 3-dB attenuators are inserted to limit the input power of the QPA9501 below the absolute maximum rating.

A BW-S3W10 + dc – 12.4-GHz 3-dB 10-W attenuator is inserted between the DUT and the injection amplifier to improve matching and to introduce losses between the DUT and the injection amplifier, ensuring stable impedance synthesis. Additional fixed attenuators—FW-6A+ (6 dB, dc –12 GHz), and VAT-20A+ (20 dB, dc –6 GHz)—are placed between the directional couplers and the ADC inputs to bring signal levels within the ADC's operating range.

All components are interconnected using coaxial cables and mounted, as shown in Fig. 2. The system operates in an open-loop configuration, where the reflected wave is synthesized using a second DAC and PA. Only a dc power supply for the amplifiers and a power meter for calibration are required externally. System control and calibration routines are implemented in MATLAB and run on a host PC communicating with the RFSoC board over TCP/IP.

The proposed setup employs DDS-based waveform generation, requiring filters to suppress image frequencies. The DACs have a maximum sampling rate of 10 GSPS, while the ADCs operate at 2.5 GSPS, limiting the simultaneous bandwidth for multitone or modulated signals to ~1.25 GHz; however, single-tone signals can be generated in the second Nyquist zone of the DACs and downsampled by ADCs, as we did in this letter, thus extending the frequency range of the setup. However, to operate above 6 GHz, external baluns are required. Both DACs and ADCs feature 14-bit resolution, corresponding ideally to a dynamic range of ~86 dB, although it degrades quickly with frequency and depends strongly on external analog components. Due to data transfer between MATLAB and the RFSoC, each measurement currently requires approximately 9 s. Also, the Smith chart coverage is limited at high power levels because the DUT and the injection amplifier have similar output capabilities, so the injection PA cannot fully synthesize high reflection coefficients when the DUT is driven near saturation.

III. Calibration

Initial calibration is performed using two-port SOLT with an unknown thru [7], followed by power calibration with an R&S NRP33SN power meter. During this step, the power meter is connected in place of the DUT, and a power sweep is performed. A calibration coefficient is then introduced to minimize the difference between the power readings of the RFSoC and the power meter. While this suffices for vector network measurements, load–pull presents additional challenges. Mismatch between the DUT and injection amplifier outputs causes multiple reflections between them, unknown cable length between the DACs and the DUT ports affects the initial phases of the signals, and nonlinear behavior of both DUT and injection amplifier alters wave amplitudes and phases dynamically, complicating the synthesis of specific load impedances.

These effects prevent direct control over the presented impedance using only the programmed DAC waveforms. Commonly, the iterative techniques, such as Newton–Raphson, are employed to compensate for that [8].

To address this, we implement a simple in situ calibration model that accounts for multiple reflections between the DUT and the injection amplifier. For the simplest case, where both DUT and the injection amplifier are assumed to be linear, the total incoming (a_2) and outgoing (b_2) waves at the DUT interface can be expressed as a sum of geometric series

$$a_2 = \frac{a_2^{\text{inc}} + a_1^{\text{inc}} S_{21}^{\text{DUT}} \Gamma_{\text{PA}} \alpha^2 e^{-j2\Delta\phi}}{1 - S_{22}^{\text{DUT}} \Gamma_{\text{PA}} \alpha^2 e^{-j2\Delta\phi}} \tag{1a}$$

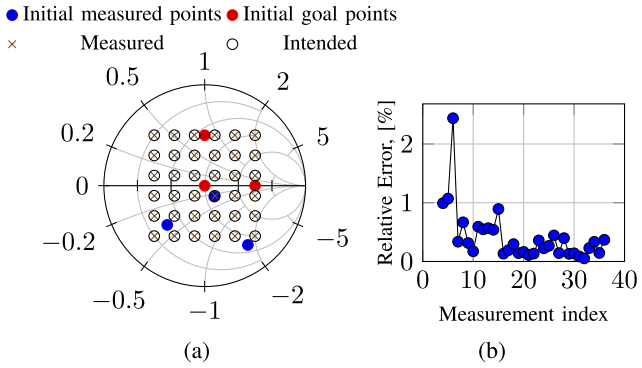

Fig. 3. Model accuracy and comparison to measured data. (a) Synthesized Γ_{Load}. (b) Relative error in reflection coefficient synthesis.

$$b_2 = \frac{a_2^{\text{inc}} S_{22}^{\text{DUT}} + a_1^{\text{inc}} S_{21}^{\text{DUT}}}{1 - S_{22}^{\text{DUT}} \Gamma_{\text{PA}} \alpha^2 e^{-j2\Delta\phi}} \tag{1b}$$

where a_i^{inc} are the incident voltage waves, synthesized by the DACs on the terminals of the DUT, S_{21}^{DUT} and S_{22}^{DUT} are the S-parameters of the DUT, Γ_{PA} is the reflection coefficient of the injection amplifier, and $\alpha e^{-j\Delta\phi}$ is the attenuation and phase shift that signal experiences traveling once from DUT to the injection amplifier.

The measured load reflection coefficient seen by the DUT is then

$$\Gamma_{\text{Load}} = \frac{b_2}{a_2} = \frac{a_2^{\text{inc}} S_{22}^{\text{DUT}} + a_1^{\text{inc}} S_{21}^{\text{DUT}}}{a_2^{\text{inc}} + a_1^{\text{inc}} S_{21}^{\text{DUT}} \Gamma_{\text{PA}} \alpha^2 e^{-j2\Delta\phi}}. \tag{2}$$

Introducing programmed reflection coefficient $\Gamma_{\text{set}} = a_1^{\text{inc}}/a_2^{\text{inc}}$ and unknown parameters $\{\alpha_n\}_{n=0}^{2}$, the load reflection coefficient seen by the DUT becomes

$$\Gamma_{\text{Load}} = \frac{\alpha_0 + \alpha_1 \Gamma_{\text{set}}}{1 + \alpha_2 \Gamma_{\text{set}}}. \tag{3}$$

Because the parameters of the DUT are functions of a_1^{inc}, this model has to be separately fitted for different input power levels. Also, to take into account the power dependency of the parameters of the injection amplifier, the corresponding coefficient in (2) can be expressed as a power series of a_2^{inc}.

Fitting is done during measurements using MATLAB's `lsqnonlin`, initialized from three calibration points: $\Gamma_{\text{set}} = 0$, 0.5, and $0.5j$. The calibration points should be well distributed across the Smith chart to minimize the influence of measurement noise on the optimized coefficients. As shown in Fig. 3, after calibration, relative error drops to sub-2.5% and is less than 0.5% on average. The measurement index is just a running counter across all measurements.

We define: "Relative error" = $|\Gamma_{\text{measured}} - \Gamma_{\text{goal}}|/|\Gamma_{\text{goal}}| \times 100\%$, and "Absolute error" = $|\Gamma_{\text{measured}} - \Gamma_{\text{goal}}|$, where Γ_{measured} is the load reflection coefficient measured by the RFSoC and Γ_{goal} is the programmed value after calibration.

Also, as can be seen from Fig. 4, the absolute error in synthesized Γ grows on the edge of the Smith chart. Relative error, on the other hand, grows drastically in the center of the Smith chart, due to division by 0. Excluding the center of the Smith chart, relative error is below 2% with a couple of points at 4%, and in absolute values, error is below 0.03 throughout the whole Smith chart.

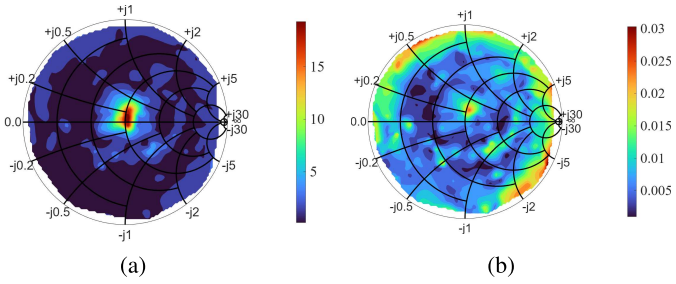

Fig. 4. Measured error depending on the position on the Smith chart. (a) Relative error [%]. (b) Absolute error.

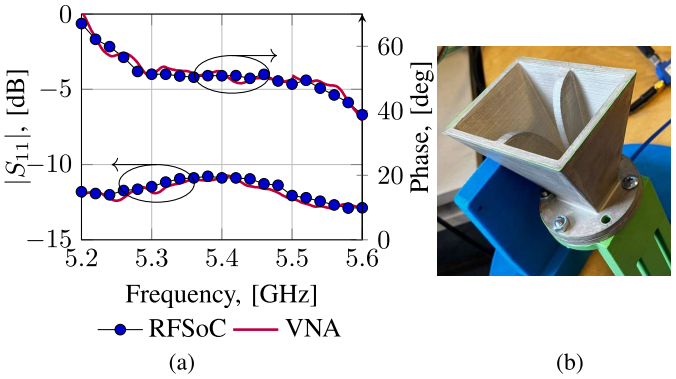

Fig. 5. Horn antenna. (a) S_{11} magnitude and phase. (b) Photograph of the horn.

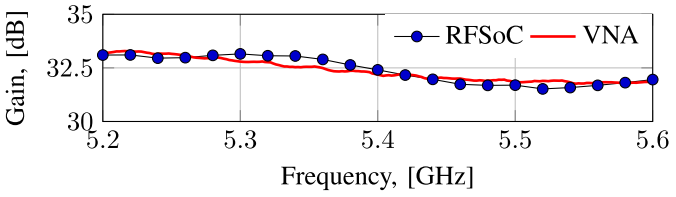

Fig. 6. Small-signal gain of the PA.

IV. Example Measurements

The setup was evaluated in two modes: as a VNA and as an active load–pull system.

Fig. 5 shows the measured return loss of a 3-D-printed horn antenna. The calibration plane was de-embedded using a port extension to remove the effect of the connecting cable. The deviation from VNA measurements is below 0.5 dB and is primarily caused by standing waves between the antenna and the room ceiling.

To verify that our measurement setup is working correctly, we also measured the small-signal gain of the off-the-shelf PA (QPA9501). Fig. 6 shows the result, which agrees well with the datasheet and with VNA measurements reaching a maximum of 0.5-dB difference.

Finally, we performed load–pull measurements at 5.4 GHz. The results are shown in Fig. 7, where (a) shows the power-added efficiency (PAE) and (b) shows the output power. These contours help identify the optimal load conditions: the highest PAE occurs near $41.7 - j13.2\ \Omega$, while the maximum output power is achieved near $32.2 - j11.3\ \Omega$. This behavior is expected because the PA is overdriven, which causes the

TABLE I
COMPARISON OF THE PROPOSED RFSOC LOAD–PULL SETUP WITH PUBLISHED SETUPS

System	External RF Instruments	maximum frequency range [GHz]	Measurement time [s]	Smith chart coverage, [%]	Power handling capability, [dBm]	Tone capability	Estimated cost
Proposed system	None	0–8 (Requires sub-band filters)	9	100	27	single tone	$20k
System in [4]	R&S RTO1044 Oscilloscope, Keysight M8190 AWG	0–4	N/A	100	45	two-tone	$100–200k
System in [6]	Ceyear 3672D VNA, Agilent 8267D signal generator	0–3.8	Real-time	100	N/A	multi-band	$100–200k

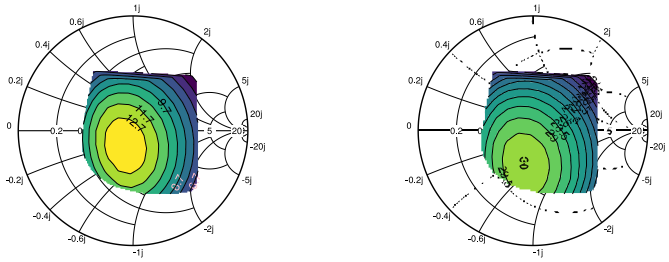

(a) (b)

Fig. 7. Load–pull contour plots. (a) PAE and (b) output power.

optimal impedance for both PAE and output power to shift slightly away from 50 Ω.

To place the proposed approach in context, Table I summarizes the instrumentation requirements and cost compared with some published load–pull solutions.

V. CONCLUSION

In this letter, we have presented a compact active open-loop load–pull measurement system built on a single RFSoC evaluation board. The system requires no external RF instrumentation, relying solely on the RFSoC itself and controlled from MATLAB on the user's PC.

We demonstrated that this architecture allows for flexible and cost-effective characterization of both active and passive RF components. A simple yet effective calibration method was proposed to compensate for unknown reflections and nonlinearities in the measurement path. The model-based approach enables accurate load synthesis without prior knowledge of the DUT.

The system's capabilities were verified through example measurements, including both antenna characterization and load–pull of a commercial RF PA. The results confirm the validity and usefulness of the setup for practical measurements, demonstrating that the system enables affordable and portable RF testing suitable for both research and education.

REFERENCES

[1] Z. Zhang et al., "6G wireless networks: Vision, requirements, architecture, and key technologies," *IEEE Veh. Technol. Mag.*, vol. 14, no. 3, pp. 28–41, Sep. 2019.

[2] R. Argaez-Ramirez, J.-R. Perez-Cisneros, and C. Fager, "Investigation of power amplifier performance under load mismatch conditions," in *Proc. IEEE Topical Conf. RF/Microw. Power Model. Radio Wireless Appl. (PAWR)*, Jan. 2021, pp. 41–43.

[3] D. Nopchinda and K. Buisman, "Measurement technique to emulate signal coupling between power amplifiers," *IEEE Trans. Microw. Theory Techn.*, vol. 66, no. 4, pp. 2034–2046, Apr. 2018.

[4] S. Gustafsson, M. Thorsell, and C. Fager, "A novel active load-pull system with multi-band capabilities," in *Proc. 81st ARFTG Microw. Meas. Conf.*, Jun. 2013, pp. 1–4.

[5] M. S. Hashmi, A. L. Clarke, S. P. Woodington, J. Lees, J. Benedikt, and P. J. Tasker, "An accurate calibrate-able multiharmonic active load–pull system based on the envelope load–pull concept," *IEEE Trans. Microw. Theory Techn.*, vol. 58, no. 3, pp. 656–664, Mar. 2010.

[6] Z. Liu, J. Su, H. Li, S. Shao, and Z. Wu, "A novel digital two-tone load-pull architecture for assessing RF device nonlinear behavior," in *Proc. Int. Conf. Microw. Millim. Wave Technol. (ICMMT)*, May 2024, pp. 1–3.

[7] T. Reveyrand, S. Hernandez, S. Mons, and E. Ngoya, "SOLT and SOLR calibration methods using a single multiport 'thru' standard connection," in *Proc. 95th ARFTG Microw. Meas. Conf. (ARFTG)*, Aug. 2020, pp. 1–4.

[8] M. Thorsell and K. Andersson, "Fast multiharmonic active load–pull system with waveform measurement capabilities," *IEEE Trans. Microw. Theory Techn.*, vol. 60, no. 1, pp. 149–157, Jan. 2012.